Characteristics of Tsunami-Affected Areas in Moderate-Resolution Satellite Images

Ken'ichi Kouchi and Fumio Yamazaki, *Member, IEEE*

***Abstract*—The massive 2004 Indian Ocean tsunami caused vast devastation along the coastal areas in countries around the Indian Ocean rim. Satellite images of various spatial resolutions could quickly capture the affected areas and were used for emergency response after the catastrophe occurred. To figure out the extent of affected areas, moderate-resolution satellites (e.g., Terra-ASTER) images are more suitable than high-resolution satellites (e.g., Ikonos) images. Basically, tsunami-affected areas can be observed and detected through land cover changes. Based on the nature of the tsunami attack, we chose the normalized difference vegetation index, soil index, and water index as indicators to help detect changes. This paper first investigates the fluctuations of these indexes and their differences using ASTER images of southern Thailand. The investigation is carried out in two cases: one using only the data acquired after the tsunami, and the other using both data acquired before and after the tsunami. Consequently, the thresholds of index differences are set up for the detection of tsunami-affected areas. In addition, since landform is a significant factor to determine the extent of tsunami runup, Shuttle Radar Topography Mission data are employed to perform geomorphological classification and to assess its relationship with the tsunami-affected areas.**

***Index Terms*—Landform classification, normalized difference vegetation index (NDVI), Terra-ASTER, the 2004 Indian Ocean tsunami, tsunami runup.**

I. Introduction

RAPID DECISION making and information gathering are crucial in the response after the occurrence of a disaster. As the damage spreads extensively, information gathering becomes more difficult. Fortunately, remote sensing is a capable technique to capture the damage information over a large area. In the past, satellite sensors provided rather coarse spatial resolution images. Hence, aerial photographs were mainly employed in gathering detailed information, like the damage caused to buildings due to an earthquake [1]. However, the recent very high resolution satellite images, like QuickBird or Ikonos, can be used in performing the same task [2]. It is also noted that the spectral and temporal resolutions of moderate-resolution satellite sensors have also been improved. For instance, Terra-ASTER sensor provides 14-channel data and most sensors can capture a target area within a few days after a catastrophe has occurred. These advances strengthen their capability in postdisaster response.

Immediately after the 2004 Indian Ocean tsunami, a large volume of remotely sensed images before and after the tsunami were delivered under the International Charter "Space and Major Disasters" [3], and they were effectively used in rescue and rehabilitation actions. In most cases, analysts and decision makers prefer very high resolution satellite images like Ikonos and QuickBird. In fact, it has been demonstrated that the damage of even individual buildings could be identified from those images although the building damage level judged from vertical images tends to be relatively lower than actual damage levels [4]. The damage level due to this tsunami in Sri Lanka has been assessed using those data [5]. Alternatively, moderate-resolution satellite (e.g., Terra-ASTER) images are necessary to assess the extensive damage distribution because of their wider coverage. It is particularly helpful in emergency management such as relief logistics. It is noted that the utilization of both resolution images for the detection of tsunami-affected areas has been proposed [6].

As a matter of fact, tsunamis attack coastal areas and wash away vegetation and other structures along the coastline. The damage extent depends on the mechanism of an earthquake, which triggers tsunamis, and also on the landform of coastal areas. Due to tsunamis, soil is more exposed as vegetation is washed away and soil moisture increases drastically. A field survey was conducted in February 2005 to observe hard-hit areas by the tsunami in southern Thailand with GPS cameras and a handheld spectrometer [7]. The results confirmed that the identification of tsunami-inundated areas can be performed through the changes in spectral indexes, which are related to vegetation, soil, and water.

This research intends to find out a set of parameters which can be used to quickly detect tsunami-inundated areas from ASTER images. ASTER images are chosen because of its reasonable spatial resolution and spectral resolution. In addition, its capability of pointing up to 24° increases its temporal resolution. First, the fluctuations of the normalized difference vegetation index (NDVI), soil index (NDSI), and water index (NDWI) are rigorously investigated. Second, the thresholds to divide tsunami-affected and nonaffected areas are set up. The effects of clouds/shadows and seasonal/man-made changes are also investigated. Landform is also taken into account to supplement the spectral reflectance. Landform is classified using Shuttle Radar Topography Mission (SRTM) data, which is also at a reasonable spatial resolution. Consequently, it is possible

Manuscript received May 2, 2006; revised September 21, 2006.

K. Kouchi is with the Transportation Planning Department, Nippon Koei Company, Ltd., Tokyo 102-8539, Japan (e-mail: a6302@n-koei.co.jp).

F. Yamasaki is with the Department of Urban Environment Systems, Faculty of Engineering, Chiba University, Chiba 263-8522, Japan (e-mail: yamazaki@tu.chiba-u.ac.jp).

Digital Object Identifier 10.1109/TGRS.2006.886968

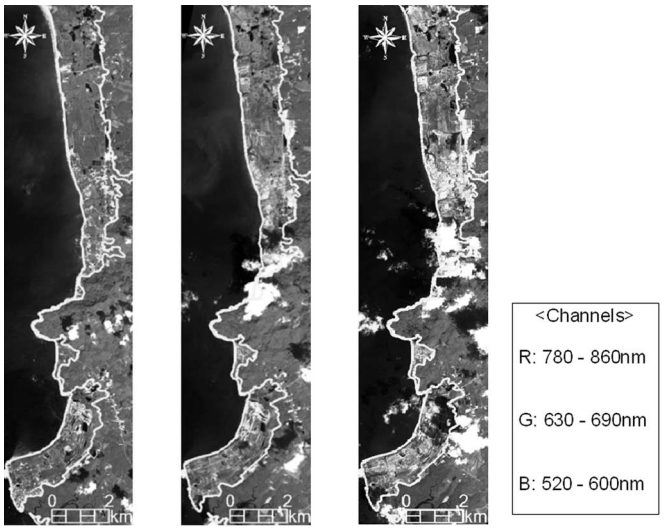

Fig. 1. ASTER false color composite images. (Left) November 15, 2002. (Middle) December 31, 2004. (Right) February 8, 2005.

to assess the relationship between landform characteristics and tsunami-inundated areas.

II. Basic Procedure

A. Data Used

ASTER is a multispectral sensor on board Terra satellite. This moderate-resolution sensor provides visible and near-infrared bands data with 15-m resolution and the short-wavelength-infrared (SWIR) band data with 30-m resolution. ASTER images of 2B05 product (http://www.gds.aster.ersdac.or.jp/gds_www2002/index_j.html) in false color composite of the study area are shown in Fig. 1. A hard-hit area in Phang-nga province, southern Thailand, was selected as the study area.

After the 2004 Indian Ocean tsunami, Geo-Informatics and Space Technology Development Agency (GISTDA), Thailand, visually captured the affected areas in southern Thailand using various multitemporal and multiresolution images [8]. The yellow lines drawn over ASTER images in Fig. 1 show these areas, which are used as the truth data in this paper. Several other high-resolution satellite images, such as QuickBird and Ikonos, were also available from various sources, e.g., Disasters Charter (http://www.disasterscharter.org./). In this paper, Ikonos images provided by GISTDA were used for reference only as we focused on developing a quick detection method using moderate-resolution satellite images.

Digital elevation model (DEM) is now publicly available at 3-arcsecond sampling for most parts of the world including Thailand (ftp://e0srp01u.ecs.nasa.gov/srtm/). This data was generated by SRTM launched on February 11, 2000 [9] and is referred to as SRTM-3 data. The data set is sometimes called "90 m data" since 3 arc second at the equator corresponds to roughly 90 m in horizontal extent. SRTM-3 data was employed in this paper to perform landform classification. Rabus *et al.* [10] discussed in detail on the accuracy of SRTM data. Based on their examination, we concluded that SRTM has enough horizontal accuracy and relative vertical accuracy to be used in our landform classification.

B. Indexes to Detect Affected Areas

The NDVI is calculated as

$$\text{NDVI} = (\text{NIR} - R)/(\text{NIR} + R) \tag{1}$$

where R and NIR are the reflectance of the red and near-infrared bands, respectively. NDVI is a simple and reliable index to identify the existence of vegetation, and therefore widely applied to assess the characteristics of the earth surface. It has been shown that not only the near-infrared and red bands but also the SWIR band (1600–1700 nm) is useful, especially for quantitatively evaluating the water content of the land surface [11]. In order to develop the indexes to identify main land cover classes like vegetation, soil, and water, Takeuchi and Yasuoka [12] have proposed the normalized difference soil and water indexes (NDSI and NDWI) by extending the idea of NDVI using the SWIR band as well as the near-infrared and red bands. NDSI and NDWI are calculated as

$$\text{NDSI} = (\text{SWIR} - \text{NIR})/(\text{SWIR} + \text{NIR}) \tag{2}$$

$$\text{NDWI} = (R - \text{SWIR})/(R + \text{SWIR}). \tag{3}$$

As mentioned above, it should be possible to identify tsunami-inundated areas using these indexes. Arakawa *et al.* [13] has demonstrated this possibility but through visual detection only. In this paper, we extend the idea further to an automated detection of tsunami-affected areas based on these indexes.

C. Processing Flowchart

The flowchart of this paper is shown in Fig. 2. As optical satellite images are affected by cloud cover, especially in tropical regions, land cover classification is carried out first in order to identify and correct cloud and shadow affected areas. Subsequently, the NDVI, NDSI, and NDWI are computed. Then, the characteristics of these indexes in tsunami-affected and nonaffected areas or in pre- and posttsunami images are compared to investigate their possibility in identifying tsunami-affected areas. The truth data is required for this purpose. In southern Thailand, we use the affected areas, which were extracted based on multitemporal and multiresolution imagery [8].

The relationship between tsunami-affected areas and landform is also assessed. The 90-m resolution SRTM data are used to derive the topographic features like gradient and ridgelines. Landform classification based on topographic features is carried out prior to the assessment. The landform classes are statistically summarized in tsunami-affected areas, which are identified based on the indexes from the ASTER image, and nonaffected areas. The details of this procedure are discussed in the next section.

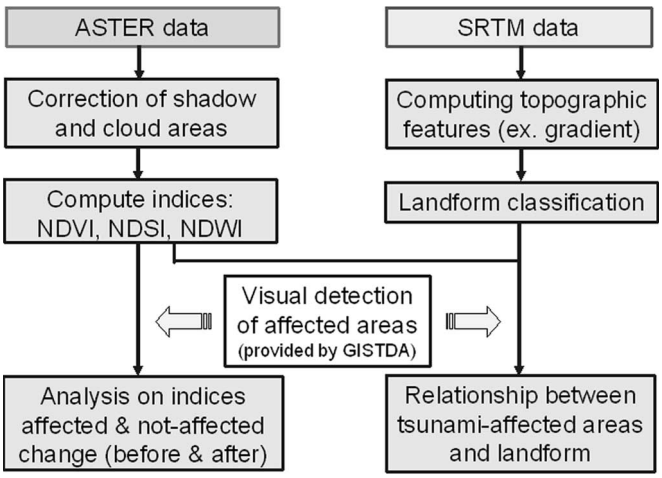

Fig. 2. Flowchart of the study.

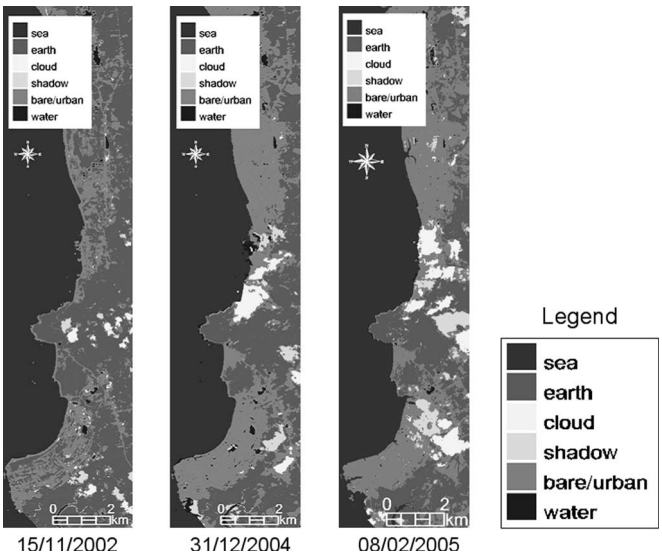

Fig. 3. Results of classification.

III. Analysis of Data Acquired Over Southern Thailand

A. Correction of Shadow and Cloud Areas

Completely cloud-free remote sensing images are not often available, especially in tropical or humid climates. However, a method to reduce the effect of clouds and shadows has rarely been studied. Song and Civco [14] conducted a knowledge-based approach for reducing the effects of clouds and shadows using two multitemporal images. Since our objective is to develop a quick detection method, we introduce a simple idea to correct cloud and shadow areas from only one image as follows.

First, ASTER images before and after the disaster are classified by a maximum-likelihood classifier using the visible and near-infrared bands into sea, cloud, shadow, water, bare/urban, and others, named earth, as shown in Fig. 3. Second, the cloud and shadow pixels are corrected following the method stated below.

Scanning from the top left to the bottom right of an image is carried out to find a cloud pixel. At this found cloud pixel, the mean value of its neighboring pixels (within a 5×5 window) that are not classified as cloud, shadow or water is calculated. The window size was determined after some trials. Then, the pixel is replaced by that mean value. This pixel shall be used for the calculation of mean values of cloud pixels found hereafter. The computation of the mean value and the replacement are repeated to the next found cloud pixel until all the cloud pixels have been replaced. In this method, cloud pixels are reduced from the upper left corner to the bottom right corner in each cloud covered area, and hence, this method has a drawback that the correction result is influenced by the position of the first cloud pixel.

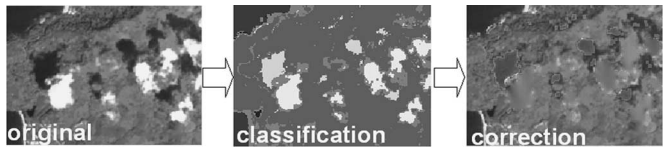

Fig. 4. Example of cloud and shadow correction.

The correction of shadow pixel values is also carried out in the similar manner. When a shadow pixel is found, the major class of its neighboring pixels (within a 5×5 window), which is thought to be the original class in the shadow pixel, is determined. Then, the pixel is reassigned to this major class. The replacement is repeated to all found shadow pixels in the image. Subsequently, the mean value of each land cover class on each spectral band is calculated in which separate calculation is conducted for areas without and with shadow. Finally, the ratios between shadow-free areas and shadow areas are computed for each land cover class. Then, the value of a shadow pixel is multiplied by the selected ratio depending on its above-assigned class.

The correction processes for clouds and shadows are different because for clouds, the correction is pure inference from the surroundings while for shadows, the correction is amplifying the reduced pixel values using the surroundings. An example of the result of classification and correction is shown in Fig. 4. The correction does not look very perfect but has a reasonable level of accuracy to employ the result in the further steps. We believe these corrections are necessary to fully utilize available data as much as possible. Note that the accuracy of land cover classification conducted before the correction needs to be high to use surrounding data for the inference of pixel values of cloud/shadow areas.

B. Computation of the Indexes

Following (1)–(3), the NDVI, NDSI, and NDWI were computed as shown in Fig. 5. The greater the NDVI is, the more vegetation covers. It is also the case with the NDSI for soil and the NDWI for water. Fig. 5 shows that, in general, NDVI decreases, and NDSI and NDWI increase in the tsunami-affected areas. These observations are based on the facts that the vegetation was washed away or became dead/weakened, soil was exposed, and the soil moisture was increased due to the tsunami.

In other words, the results demonstrate a clear difference in the indexes for the affected areas before and after the disaster and a difference between the affected areas and the other areas

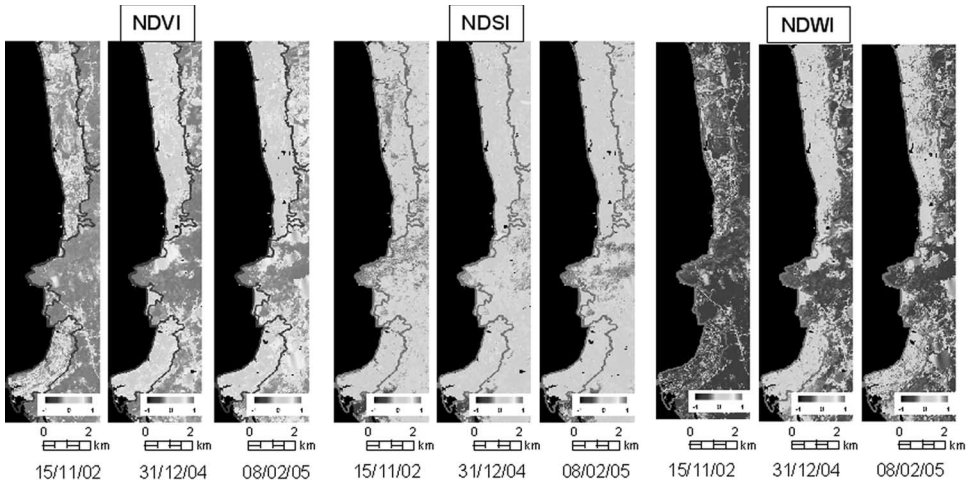

Fig. 5. Computed NDVI, NDSI, and NDWI for preevent and postevent ASTER images.

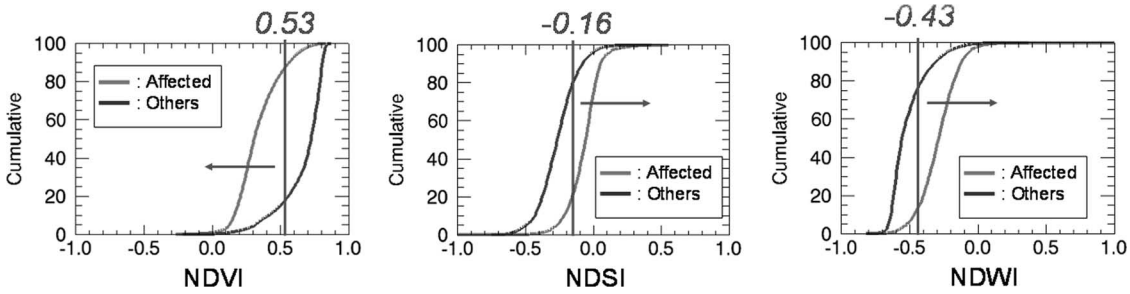

Fig. 6. Cumulative frequency distributions of NDVI, NDSI, and NDWI from the data one week after the tsunami.

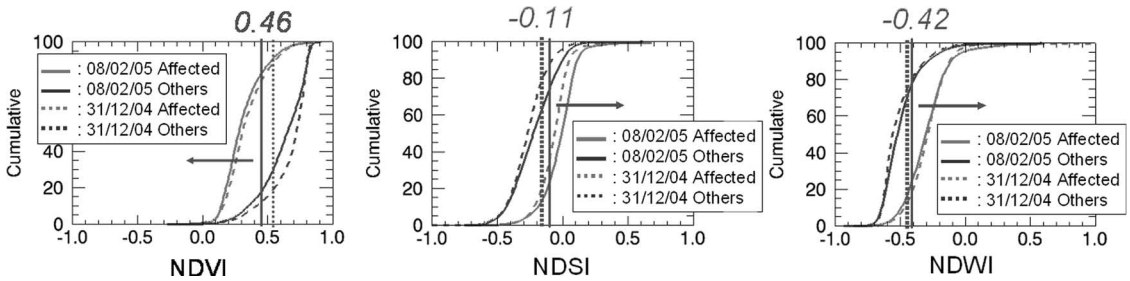

Fig. 7. Comparison of cumulative frequency distributions of the indexes between one week and one month after the tsunami.

after the disaster. These differences could be good indicators of tsunami inundation. More rigorous analysis on the characteristics of the indexes is discussed in the following section.

C. Threshold Analysis

1) Using Only the Posttsunami Image: The first analysis is to compare the characteristics of three indexes in the affected areas and nonaffected areas using only a single postevent image, and consequently, determine the thresholds for detection of tsunami-affected areas. It might be applicable in the case no preevent image exists.

The cumulative frequency distributions of NDVI, NDSI, and NDWI in the affected areas and nonaffected areas are plotted in Fig. 6. As a result, it is observed that there are clear differences in the distributions between the two plots for each index. It is possible to determine a value where the difference between their cumulative frequency distributions is maximized as a threshold to distinguish two classes. This method gives the most probable value to divide two classes in the Kolmogorov–Smirnov test [15]. Using this method, the thresholds to identify affected areas are 0.53 for NDVI, -0.16 for NDSI, and -0.43 for NDWI. To summarize, the pixels which have NDVI value less than the threshold, and NDSI and NDWI values more than the thresholds are identified to belong to tsunami-affected areas using only the postevent image.

Practically, vegetation is expected to recover after some time. However, the NDVI varies depend on the season, as seen in the nonaffected areas in Fig. 5. Moreover, the NDWI might be influenced by the weather condition and the elapsed time after the tsunami. A further analysis compares the cumulative frequency distributions of the indexes between one week and one month after the tsunami in Fig. 7. The distributions of NDVI and NDSI show that vegetation was further weakened one month after the tsunami. On the other hand, the NDWI in "the affected areas" slightly decreased while the one in

"non-affected areas" slightly increased. It implies that after one month, water carried by the tsunami evaporated and soil moisture in the tsunami-affected areas decreased.

To use these indexes in the detection of tsunami-affected areas, their annual fluctuations should be evaluated beforehand. The determined thresholds should be adjusted to reflect the seasonal vegetation characteristics in the further study. Furthermore, it has to be ensured that indexes give clear differences between affected areas and other areas. It seems that the alternative solution using the difference of these indexes between pre- and postevent data as the indicators of the effects of tsunami might be more reliable.

2) Using Both the Pretsunami and Posttsunami Images: For moderate resolution satellite images like Terra-ASTER, preevent images of a target area exist with high probability, even though the acquired season is not the same. Hence, the comparison of pre- and postevent images is considered to be more robust than using only a postevent image. As mentioned before, since the significant changes of the NDVI, NDSI, and NDWI values in the tsunami-affected areas are seen in Fig. 5, it might be possible to identify tsunami-affected areas by taking the difference of the indexes computed from the preevent and postevent images.

The image acquired on November 15, 2002 was used as the preevent one and the image acquired on December 31, 2004 was used as the postevent one. It is obvious that using an image of a year before is much simple and better for change detection due to a tsunami. However, unfortunately, such images do not exist in most cases, which is often the case in tropical regions due to cloud cover.

First, the pixels with NDVI less than 0.61, which is 20 percentile of its cumulative frequency distribution in the affected areas based on the preevent image, were excluded. In other words, we focused on the pixels showing high possibility of the existence of vegetation. The difference of NDVI between the pre- and postevent images was computed only with the pixels where NDVI is greater than 0.61 before the tsunami. For the NDSI and NDWI indexes, on the contrary, only the pixels where the indexes are less than -0.21 and -0.43, which are 80 percentile of their cumulative frequency distributions based on the preevent image, were used.

Second, after a simple subtraction of the indexes between the pre- and postevent images, the seasonal effect could be evaluated. They were derived from the differences between the average values in the nonaffected areas before and after the tsunami. These differences are -0.093, 0.078, and 0.067 for NDVI, NDSI, and NDWI, respectively. After eliminating the seasonal effect, the indexes' differences are illustrated in Fig. 8. In the figure, white pixels were excluded from the following process because they have less than 20 percentile value for NDVI or more than 80 percentile value for NDSI or NDWI, as stated above.

Fig. 8 shows rather big changes of the values in the tsunami-affected areas. There are also obvious changes, especially for NDVI and NDSI, in the nonaffected areas. In these areas, NDVI decreased and NDSI increased. Visual inspection as the one shown in Fig. 9 using Ikonos image shows that there was the land use change (tree cutting). Another evidence for this

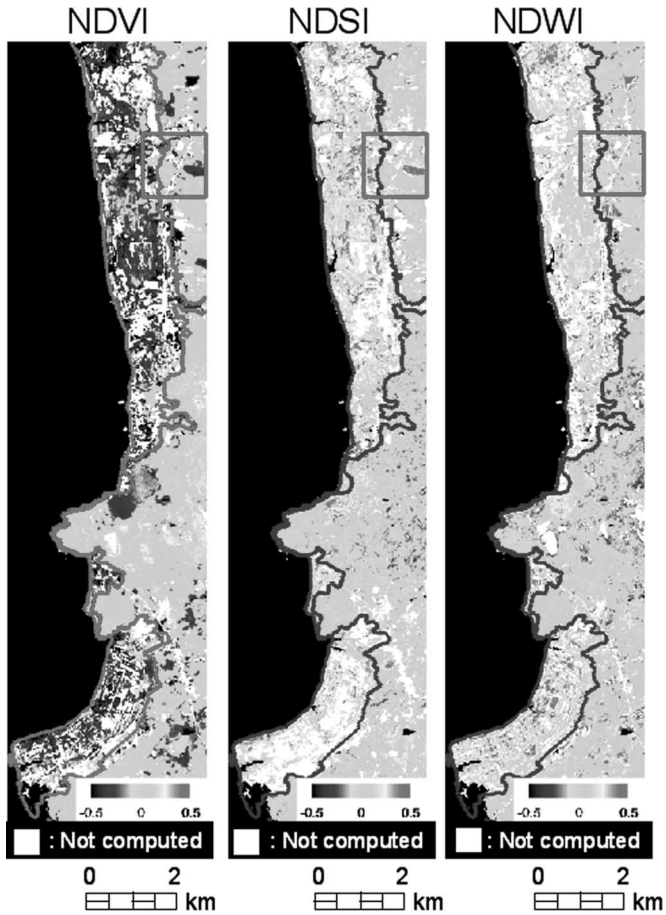

Fig. 8. Differences of the indexes between the pre- and postevent data.

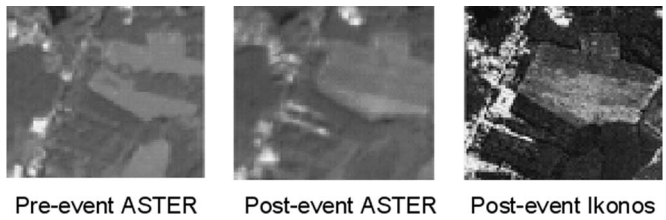

Fig. 9. ASTER and Ikonos images of the area with a man-made land use change. The area is the detail of the square in the upper part of Fig. 8.

observation is that these areas have straight boundaries, i.e., man made.

Subsequently, the distribution of the indexes' differences in the affected and nonaffected areas was calculated. The cumulative frequency distributions of the time differences of NDVI, NDSI, and NDWI in the affected and nonaffected areas are plotted in Fig. 10. Similarly to the detection using only the postevent image, the thresholds for detecting tsunami-affected areas were determined. In summary, the pixels which have the NDVI difference less than the threshold, and the NDSI and NDWI differences more than the thresholds are identified as tsunami-affected areas in tsunami damage detection based on the pre- and postevent images.

D. Topographic Features and Landform Classification

To investigate the relationship between landform characteristics and tsunami inundation, landform classification was

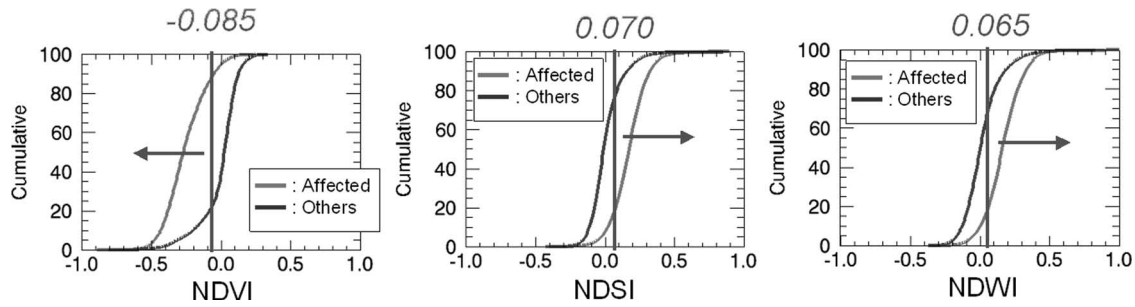

Fig. 10. Cumulative frequency distributions of the differences of NDVI, NDSI, and NDWI.

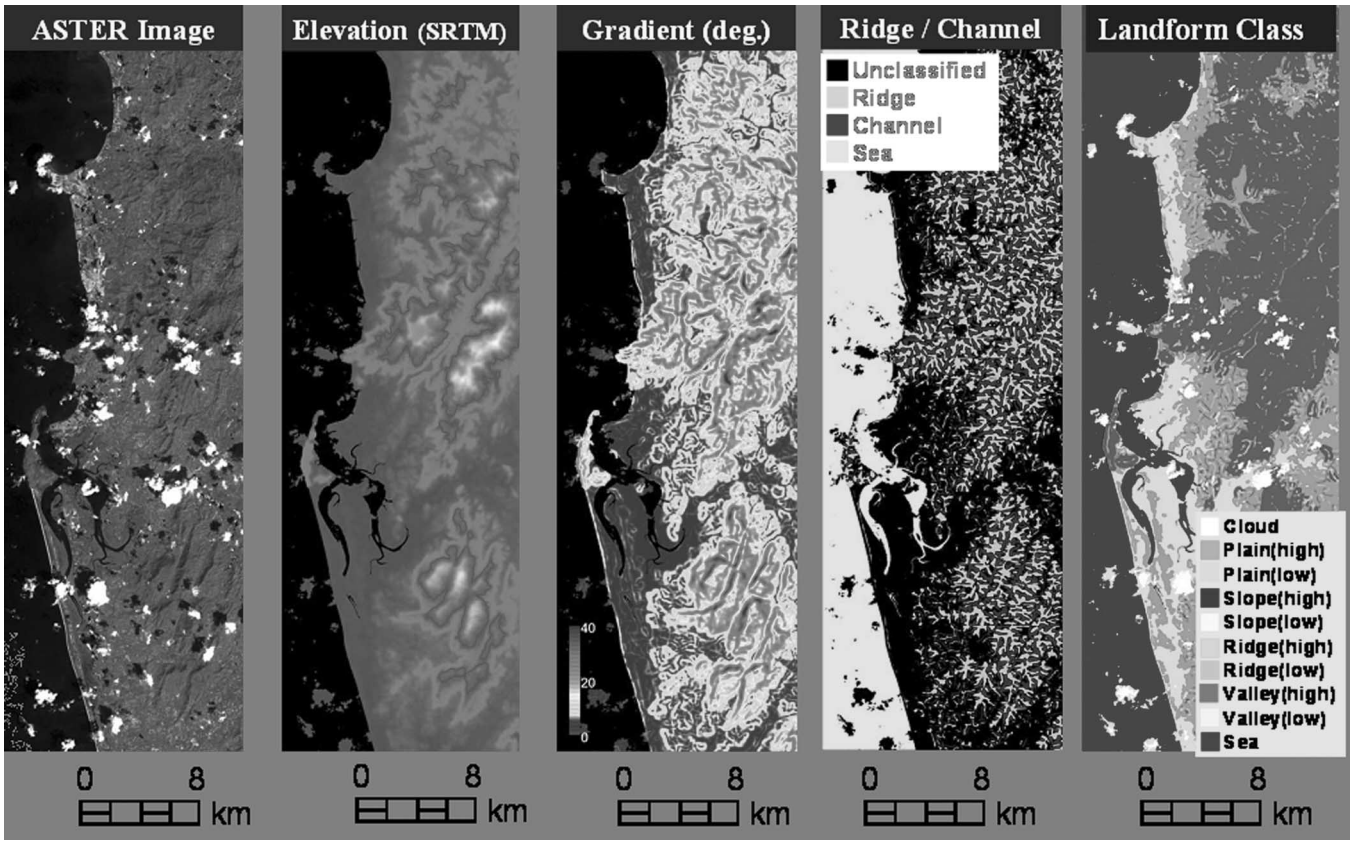

Fig. 11. Topographic features and the landform classification result in the study area.

conducted in the study area based on the SRTM data. Fig. 11 shows the ASTER image of the study area acquired on February 8, 2005 and topographic features, like an angle of gradient and ridge or channel areas of the same area, derived from the SRTM data. A landform classification result is also shown in Fig. 11, which was obtained through a decision tree method. In the reference [16], five categories of landform, which are mountain, plateau, lowland, reclaimed land, and natural levee, are suggested considering its use in the estimation of site amplification factors and the accuracy of data used. As tsunami inundation is assessed in this paper, we considered reclaimed land and natural levee as a part of lowland and added the threshold of height.

It is expected that these landform classification results depend on the DEM used. It is obvious that small landform variation within 90-m cell of SRTM-3 cannot be detected. However, we used the SRTM data only for calculating the geomorphological parameters, and hence the limitation in accuracy is not very significant.

First of all, "Sea" and "Cloud" were extracted visually from the ASTER data. Next, the rest was classified into "High" and "Low" areas based on the elevation of 10 m. Then, each class was classified as follows. "Slope (High/Low)" is a pixel with the gradient greater than 5°. A pixel with the gradient less than 5° is classified as "Plain (High/Low)" if it is not in the ridge nor channel areas. "Ridge" and "Channel" were assigned for the pixels whose gradient is greater than 1° and whose absolute cross-sectional curvature is less than 0.1, using a function in ENVI software. The summary of the classification method is demonstrated in Fig. 12, where three branches exist: i.e., "altitude," "gradient," and "the angle and direction of slope."

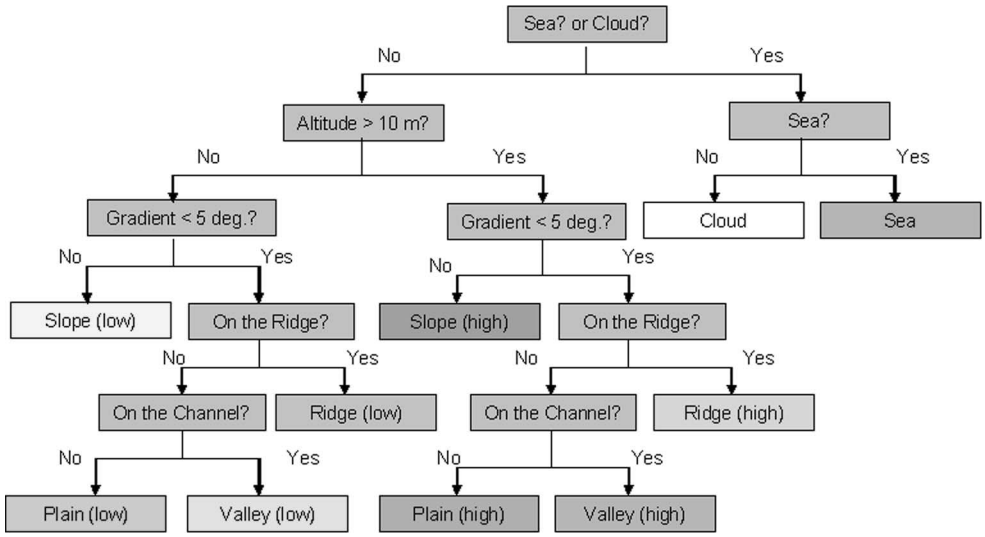

Fig. 12. Decision tree for landform classification.

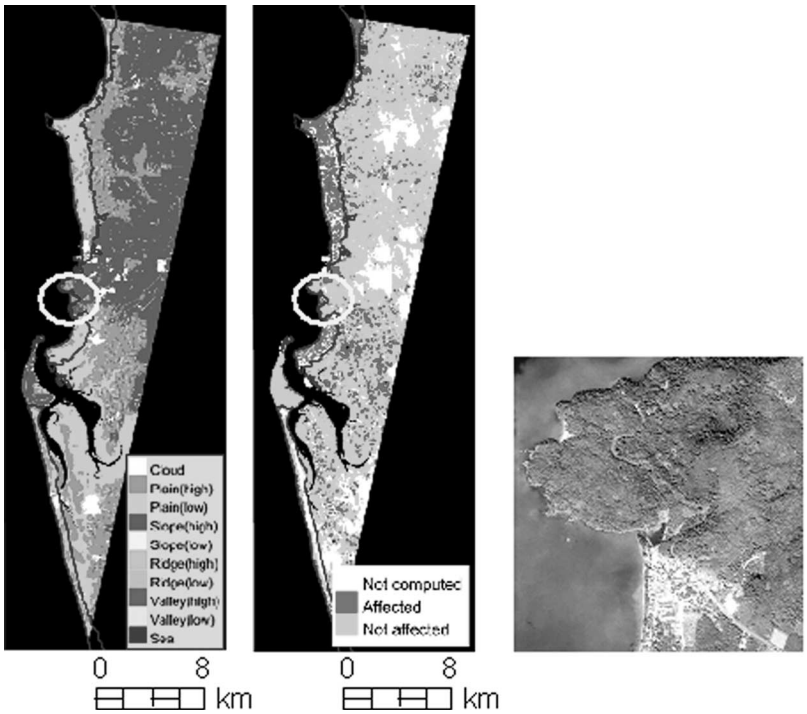

Fig. 13. Results of (left) the landform classification, (center) identified affected areas, and (right) Ikonos image of the circled area taken on December 12, 2004 (GISTDA).

E. Relationship Between Landform and the Tsunami-Affected Areas

To find out the relationship between the landform and the tsunami inundated areas, the detection of tsunami-affected areas was carried out simply using the NDVI difference data with the threshold of -0.085 as obtained in Fig. 10. The results of landform classification and detection of tsunami-affected areas are illustrated in Fig. 13. Fig. 13 is cropped from Fig. 11 so as to show the common area between the pre- and postevent images. In other wards, the preevent image does not cover such a large area as the postevent image does. Red pixels mean "Affected" pixels: the pixels with NDVI decreased more than 0.085 after the tsunami. Others are called "Not affected" pixels.

Visual inspection showed that "Affected" pixels are mainly located in the "Plain (Low)" area. However, like in a yellow circle in Fig. 13, even "Plain (High)" area was inundated by the tsunami. Based on a postevent Ikonos image and the result of our field survey, the circled area has rather low altitude, probably less than 10 m. Hence, the landform classification from 90-m SRTM data might not be very accurate, especially for small areas like this location. It is also considered that the tsunami was amplified locally because of the seabed configuration and the coastline topography there.

The areas of landform classes in "Affected" were summed up. It is observed that about 70% of the affected areas are "Plain (low)" and about 21% are "Plain (high)." Obviously, most "Affected" pixels in "Plain (high)" class have been misclassified. The distance from the coastline and other topographic conditions should also be considered for more detailed explanation of tsunami inundation areas, however. It is also desirable to employ a DEM with higher resolution than 90-m SRTM data in the future study.

IV. Conclusion

The fundamental analysis toward tsunami-damage detection using moderate-resolution satellite imagery for the areas hit by the 2004 Indian Ocean tsunami was carried out. Focusing on land cover change due to the tsunami, three indexes to indicate land cover characteristics, which are NDVI, NDSI, and NDWI, were employed in order to detect the areas affected by the tsunami. Through the analysis on these indexes, it has been demonstrated that, the tsunami resulted in the decrease of NDVI and the increase of NDSI and NDWI. The thresholds of the indexes to identify the tsunami-affected areas were determined in two cases, i.e., using only the postevent image and using both the preevent and postevent images. Comparing with the truth data provided by GISTDA, the both methods showed reasonable differences in the three indexes between the tsunami affected and nonaffected areas. This observation is, however, dependent on the environmental and climatic conditions of an affected area. It is also pointed out that the changes in the three indexes may have some correlation. Thus, the findings obtained in this paper should be examined further for some other examples.

Moreover, the relationship between landform characteristics evaluated from 90-m SRTM data and tsunami inundation areas was assessed. We found that most of pixels with NDVI greatly decreased after the tsunami are located in the low plain areas. For more detailed explanation of tsunami inundation areas, however, the distance from the coastline and other topographic conditions should also be considered as well as employing a higher resolution DEM.

Acknowledgment

The authors would like to thank S. Polngam (GISTDA, Thailand) for providing the visually detected results of tsunami-affected areas based on Ikonos images. The authors would also like to thank T. T. Vu (Chiba University) for reviewing the manuscript.

References

[1] N. Ogawa and F. Yamazaki, "Photo-interpretation of building damage due to earthquakes using aerial photographs," presented at the 12th World Conf. Earthquake Engineering, 2000, Paper 1906. CD-ROM.

[2] F. Yamazaki, K. Kouchi, M. Matsuoka, M. Kohiyama, and N. Muraoka, "Damage detection from high-resolution satellite images for the 2003 Boumerdes, Algeria earthquake," presented at the 13th World Conf. Earthquake Engineering, 2004, Paper 2595. CD-ROM.

[3] K. S. Oo, M. Mehdiyev, and L. Samarakoon, "Potential of satellite data in assessing coastal damage caused by South-Asia tsunami in December 2005—A field survey report," *Asian J. Geoinformatics*, vol. 5, no. 2, pp. 16–37, 2005.

[4] F. Yamazaki, Y. Yano, and M. Matsuoka, "Visual damage interpretation of buildings in Bam city using quickBird images following the 2003 Bam, Iran, earthquake," *Earthq. Spectra*, vol. 21, no. S1, pp. 329–336, 2005.

[5] L. K. Perera and S. Herath, "Detecting tsunami damage from satellite data in Sri Lanka," *Asian J. Geoinformatics*, vol. 5, no. 2, pp. 38–44, 2005.

[6] T. T. Vu, M. Matsuoka, and F. Yamazaki, "Dual-scale approach for detection of tsunami-affected areas using optical satellite images," *Int. J. Remote Sens.*, 2007, to be published.

[7] F. Yamazaki, M. Matsuoka, P. Warnitchai, S. Polngam, and S. Ghosh, "Tsunami reconnaissance survey in Thailand using satellite images and GPS," *Asian J. Geoinf.*, vol. 5, no. 2, pp. 53–61, 2005.

[8] S. Vibulsreth, S. Ratanasermpong, and S. Polngam, "Tsunami disasters along the Andaman Sea, Thailand," *Asian J. Geoinf.*, vol. 5, no. 2, pp. 3–15, 2005.

[9] T. Farr and M. Kobrick, "The Shuttle Radar Topography Mission produces a wealth of data," *Trans. Amer. Geophys. Union EOS*, vol. 81, no. 48, pp. 583–585, 2000.

[10] B. Rabus, M. Eineder, A. Roth, and R. Bamler, "The Shuttle Radar Topography Mission—A new class of digital elevation models acquired by spaceborne radar," *ISPRS J. Photogramm. Remote Sens.*, vol. 57, no. 4, pp. 241–262, 2003.

[11] W. G. Cibula, E. F. Zetka, and D. L. Rickman, "Response of Thematic Mapper bands to plant water stress," *Int. J. Remote Sens.*, vol. 13, no. 10, pp. 1869–1880, 1992.

[12] W. Takeuchi and Y. Yasuoka, "Development of normalized vegetation, soil and water indices derived from satellite remote sensing data," *J. Jpn. Soc. Photogramm. Remote Sens.*, vol. 43, no. 6, pp. 7–19, 2004, (in Japanese).

[13] Y. Arakawa, M. Kato, T. Tachikawa, and K. Okada, "Terra/ASTER urgent observation of earthquake and tsunami damaged area in north Sumatra, Indonesia and data analysis by using NDXI," in *Proc. 26th Asian Conf. Remote Sens.*, 2005, CD-ROM.

[14] M. Song and D. L. Civco, "A knowledge-based approach for reducing cloud and shadow," in *Proc. 2002 ASPRS-ACSM Annu. Conf. and FIG XXII Congr.*, 2002.

[15] M. Takagi and H. Shimoda, *Handbook of Image Analysis [Revised Edition]*. Tokyo, Japan: Univ. Tokyo Press, 2004, pp. 1605–1607 (in Japanese).

[16] B. Jeong, M. Hosokawa, and S. Zama, "A study on classification of landform using remote sensing and its application to earthquake damage estimation—A classification of landform using SRTM-3 for estimation of site amplification factors," in *Proc. 2nd Asia Conf. Earthq. Eng.*, 2006, CD-ROM.

Ken'ichi Kouchi received the M.S. degree in civil engineering, focusing on the detection of damage due to earthquakes and tsunamis using remotely sensed imagery, from University of Tokyo, Tokyo, Japan, in 2006.

He is currently working for Nippon Koei Company, Ltd., Tokyo, a consulting company of civil engineering in Japan, and is mainly involved in transport planning.

Fumio Yamazaki (M'03) received the M.S. degree in 1978 and the Ph.D. degree in 1987, both in civil engineering, from the University of Tokyo, Tokyo, Japan.

He worked for Shimizu Corporation, Japan, for eight years and served as a Visiting Scholar with Columbia University, for two years. He is currently a Professor of Urban Environment Systems with Chiba University, Chiba, Japan. His research interests include stochastic engineering mechanics, earthquake engineering, and more recently, application of geographic information system (GIS) and remote sensing technologies to disaster management.